Supplemental Materials for "Polariton-drag enabled quantum geometric photocurrents in high symmetry materials"

Ying Xiong,[1] Li-kun Shi,[2] and Justin C.W. Song[1,*]

[1] *Division of Physics and Applied Physics, Nanyang Technological University, Singapore 637371*
[2] *Max Planck Institute for the Physics of Complex Systems, 01187 Dresden, Germany*

I. Geometric representation of shift and injection current

A. Geometric representation of shift current

The shift photocurrent arises from a real-space displacement $\mathbf{R}(\mathbf{k},\mathbf{q})$ when an electron undergoes interband transition, see Eq. (1) in the main text. The finite-$\mathbf{q}$ shift vector $\mathbf{R}(\mathbf{k},\mathbf{q})$ can be written as [29]

$$\mathbf{R}(\mathbf{k},\mathbf{q}) = \mathbf{A}_c(\mathbf{k}_+) - \mathbf{A}_v(\mathbf{k}_-) - \nabla_{\mathbf{k}} \arg\left[\hat{\mathbf{e}}\cdot\boldsymbol{\nu}_{cv}(\mathbf{k},\mathbf{q})\right], \tag{S1}$$

where $\mathbf{A}_n(\mathbf{k}) = \langle u_n(\mathbf{k})|i\nabla_{\mathbf{k}}|u_n(\mathbf{k})\rangle$ is the Berry connection and $\hat{\mathbf{e}}$ is the unit vector for the electric field polarisation. The shift vector is determined by the quantum geometry of the Bloch bands and the light polarisation. To see this, we rewrite $\mathbf{R}(\mathbf{k},\mathbf{q})$ as a derivative of the Pancharatnam-Berry phase obtained from the Wilson loop associated with the interband transition, as defined in Eq. (2) of the main text. To uncover the geometric meaning of the shift vector, we first note that the Berry connection can be written:

$$A_n^b(\mathbf{k}) = -\lim_{\delta k_b\to 0}\partial_{k_b}\arg\langle u_n(\mathbf{k})|u_n(\mathbf{k}+\delta k\hat{\mathbf{b}})\rangle = \lim_{\delta k_b\to 0}\partial_{k_b}\arg\langle u_n(\mathbf{k}+\delta k\hat{\mathbf{b}})|u_n(\mathbf{k})\rangle, \tag{S2}$$

where $\hat{\mathbf{b}}$ is the unit vector in direction $b=\{x,y\}$. On the other hand, the last term in Eq. S1 can be rewritten as

$$-\nabla_{\mathbf{k}}\arg\left[\hat{\mathbf{e}}\cdot\boldsymbol{\nu}_{cv}(\mathbf{k},\mathbf{q})\right] = \nabla_{\mathbf{k}}\arg\langle u_v(\mathbf{k}_-)|\hat{\mathbf{e}}\cdot\hat{\boldsymbol{\nu}}|u_c(\mathbf{k}_+)\rangle = \lim_{\delta\mathbf{k}\to 0}\nabla_{\delta\mathbf{k}}\arg\langle u_v(\mathbf{k}_-+\delta\mathbf{k})|\hat{\mathbf{e}}\cdot\hat{\boldsymbol{\nu}}|u_c(\mathbf{k}_++\delta\mathbf{k})\rangle \tag{S3}$$

Therefore, the shift vector can be expressed as the gradient of the Panchanratnam-Berry phase of the Wilson loop

$$\mathbf{R}(\mathbf{k},\mathbf{q}) = \lim_{\delta\mathbf{k}\to 0}\nabla_{\delta\mathbf{k}}\arg\mathcal{W}(\mathbf{k},\delta\mathbf{k},\mathbf{q}), \tag{S4}$$

where

$$\mathcal{W}(\mathbf{k},\delta\mathbf{k},\mathbf{q}) = \langle u_v(\mathbf{k}_-)|u_v(\mathbf{k}'_-)\rangle[\hat{\mathbf{e}}\cdot\langle u_v(\mathbf{k}'_-)|\hat{\boldsymbol{\nu}}|u_c(\mathbf{k}'_+)\rangle]\langle u_c(\mathbf{k}'_+)|u_c(\mathbf{k}_+)\rangle\langle u_c(\mathbf{k}_+)|u_v(\mathbf{k}_-)\rangle \tag{S5}$$

with $\mathbf{k}'_- = \mathbf{k}_- + \delta\mathbf{k}$, and $\mathbf{k}'_+ = \mathbf{k}_+ + \delta\mathbf{k}$. Here we have introduced $\langle u_c(\mathbf{k}_+)|u_v(\mathbf{k}_-)\rangle$ to complete the Wilson loop; we note that $\nabla_{\delta\mathbf{k}}\arg\left[\langle u_c(\mathbf{k}_+)|u_v(\mathbf{k}_-)\rangle\right] = 0$ does not contribute to the shift vector. Eq. (S4) and (S5) provide a geometric interpretation of the shift vector, which corresponds to the gradient of the Pancharatnam-Berry associated with the interband transitions.

B. Geometric representation of the injection current

In this section, we show that the injection photocurrents depend on the quantum geometric tensor of the material. To see this, we note that the injection current for an arbitrarily polarised light can be written as

$$\begin{aligned}\partial_t \mathbf{j}^{\mathrm{inj}}(\mathbf{q}) &= C\sum_{\mathbf{k},a,b}\rho(\mathbf{k},\mathbf{q})\boldsymbol{\Delta}(\mathbf{k},\mathbf{q})\nu_{cv}^b(\mathbf{k},\mathbf{q})[\nu_{cv}^a(\mathbf{k},\mathbf{q})]^* E_b E_a^* \\ &= -\frac{e^3\pi}{2\hbar}\sum_{\mathbf{k},a,b}\rho(\mathbf{k},\mathbf{q})\boldsymbol{\Delta}(\mathbf{k},\mathbf{q})Q_{ba}^{cv}(\mathbf{k},\mathbf{q})E_b E_a^*\end{aligned} \tag{S6}$$

Here we have defined $r_{cv}^a(\mathbf{k},\mathbf{q}) = \nu_{cv}^a(\mathbf{k},\mathbf{q})/[i\omega_{cv}(\mathbf{k},\mathbf{q})]$ and $\omega_{cv}(\mathbf{k},\mathbf{q}) = [\epsilon_c(\mathbf{k}_+) - \epsilon_v(\mathbf{k}_-)]/\hbar$. In the second line of Eq. S6, we have introduced the c,v band resolved $\mathbf{q}$-dependent interband quantum geometric tensor as

$$Q_{ba}^{cv}(\mathbf{k},\mathbf{q}) = r_{cv}^b(\mathbf{k},\mathbf{q})[r_{cv}^a(\mathbf{k},\mathbf{q})]^*. \tag{S7}$$

For linearly polarised light with polarisation angle θ, the injection current is determined by the real part of $Q^{cv}_{ba}(\mathbf{k},\mathbf{q})$:

$$\partial_t \mathbf{j}^{\rm inj}_\theta(\mathbf{q}) = -\frac{e^3\pi}{2\hbar}\sum_{\mathbf{k},a,b}\rho(\mathbf{k},\mathbf{q})\mathbf{\Delta}(\mathbf{k},\mathbf{q})G^{cv}_{ba}(\mathbf{k},\mathbf{q})E_bE^*_a \tag{S8}$$

with $G^{cv}_{ba}(\mathbf{k},\mathbf{q}) = \mathrm{Re}\left[Q^{cv}_{ba}(\mathbf{k},\mathbf{q})\right]$ the $\mathbf{q}$-dependent interband quantum metric. We note parenthentically that the helicity dependent circular injection current is determined by the imaginary part of the $\mathbf{q}$-dependent interband quantum geometric tensor multiplied by $\mathbf{\Delta}(\mathbf{k},\mathbf{q})$. At $\mathbf{q}=0$, this reduces to interband Berry curvature dipole for vertical transitions; this reproduces the well-known result for quantised circular injection photocurrents [2, 8].

II. Symmetry Analysis for Polariton-drag (PD) Shift and Injection Currents

In this section, we discuss the symmetry properties of photon drag shift and injection currents induced by linearly or circularly polarised light. We will demonstrate that properties of the PD injection and shift photocurrents are sensitive to the symmetry of the material irradiated as well as the light polarisation. These properties can be obtained by examining how the Bloch wavefunction and velocity matrix elements transform under various symmetry operators.

We begin with the Bloch Hamiltonian $H(\mathbf{k}) = e^{-i\mathbf{k}\cdot\mathbf{r}}\mathcal{H}(\mathbf{r})e^{i\mathbf{k}\cdot\mathbf{r}}$. The Bloch wavefunction $|u_n(\mathbf{k})\rangle$ in band n satisfies $H(\mathbf{k})|u_n(\mathbf{k})\rangle = \epsilon_{n,\mathbf{k}}|u_n(\mathbf{k})\rangle$. We proceed by considering how the Bloch hamiltonian and its associated Bloch wavefunctions transform when the material possesses (i) spatial inversion ($\mathcal{P}$) symmetry [so that $\mathcal{P}H(\mathbf{k})\mathcal{P}^{-1} = H(-\mathbf{k})$], or (ii) time-reversal ($\mathcal{T}$) symmetry [so that $\mathcal{T}H(\mathbf{k})\mathcal{T}^{-1} = H(-\mathbf{k})$] respectively.

When the material possesses spatial inversion symmetry, the Bloch hamiltonian obeys

$$\mathcal{P}H(\mathbf{k})|u_n(\mathbf{k})\rangle = \mathcal{P}H(\mathbf{k})\mathcal{P}^{-1}\mathcal{P}|u_n(\mathbf{k})\rangle = \epsilon_{n,\mathbf{k}}\mathcal{P}|u_n(\mathbf{k})\rangle = H(-\mathbf{k})\mathcal{P}|u_n(\mathbf{k})\rangle, \tag{S9}$$

yielding the following constraints on the energy dispersion and the Bloch wavefunctions:

$$\epsilon_{n,\mathbf{k}} = \epsilon_{n,-\mathbf{k}}, \quad \mathcal{P}|u_n(\mathbf{k})\rangle = C_{n,\mathbf{k}}|u_n(-\mathbf{k})\rangle, \tag{S10}$$

where $C_{n,\mathbf{k}}$ is a complex phase factor associated with the $\mathcal{P}$ transformation satisfying $|C_{n,\mathbf{k}}| = 1$. Since $\mathcal{P}$ is unitary and preserves inner product, we have

$$\langle u_n(-\mathbf{k}_1)|u_m(-\mathbf{k}_2)\rangle = \langle C^*_{n,\mathbf{k}_1}\mathcal{P}u_n(\mathbf{k}_1)|C^*_{m,\mathbf{k}_2}\mathcal{P}u_m(\mathbf{k}_2)\rangle = C_{n,\mathbf{k}_1}C^*_{m,\mathbf{k}_2}\langle u_n(\mathbf{k}_1)|u_m(\mathbf{k}_2)\rangle. \tag{S11}$$

Furthermore, under spatial inversion symmetry, the velocity operator transforms as $\mathcal{P}\hat{\boldsymbol{\nu}}\mathcal{P}^{-1} = -\hat{\boldsymbol{\nu}}$. Thus the velocity matrix element satisfies

$$\langle u_n(\mathbf{k}_1)|\hat{\boldsymbol{\nu}}|u_m(\mathbf{k}_2)\rangle = \langle u_n(\mathbf{k}_1)|\mathcal{P}^{-1}\mathcal{P}\hat{\boldsymbol{\nu}}\mathcal{P}^{-1}\mathcal{P}|u_m(\mathbf{k}_2)\rangle = -C^*_{n,\mathbf{k}_1}C_{m,\mathbf{k}_2}\langle u_n(-\mathbf{k}_1)|\hat{\boldsymbol{\nu}}|u_m(-\mathbf{k}_2)\rangle. \tag{S12}$$

In the same fashion as above, when the material possesses time-reversal symmetry, the energy dispersion and Bloch wavefunctions transform as

$$\epsilon_{n,\mathbf{k}} = \epsilon_{n,-\mathbf{k}}, \quad \mathcal{T}|u_n(\mathbf{k})\rangle = C'_{n,\mathbf{k}}|u_n(-\mathbf{k})\rangle, \tag{S13}$$

where $C'_{n,\mathbf{k}}$ is a complex phase factor associated to $\mathcal{T}$ operation with $|C'_{n,\mathbf{k}}| = 1$. In addition, since $\mathcal{T}$ is anti-unitary, the inner product of the wavefunctions satisfies

$$\langle u_n(-\mathbf{k}_1)|u_m(-\mathbf{k}_2)\rangle = \langle C'^*_{n,\mathbf{k}_1}\mathcal{T}u_n(\mathbf{k}_1)|C'^*_{m,\mathbf{k}_2}\mathcal{T}u_m(\mathbf{k}_2)\rangle = C'_{n,\mathbf{k}_1}C'^*_{m,\mathbf{k}_2}\langle u_n(\mathbf{k}_1)|u_m(\mathbf{k}_2)\rangle^*. \tag{S14}$$

The velocity operator transforms as $\mathcal{T}\hat{\boldsymbol{\nu}}\mathcal{T}^{-1} = -\hat{\boldsymbol{\nu}}$, and thus the velocity matrix element satisfies

$$\langle u_n(-\mathbf{k}_1)|\hat{\boldsymbol{\nu}}|u_m(-\mathbf{k}_2)\rangle = \langle C'^*_{n,\mathbf{k}_1}\mathcal{T}u_n(\mathbf{k}_1)|\mathcal{T}(-\hat{\boldsymbol{\nu}})\mathcal{T}^{-1}|C'^*_{m,\mathbf{k}_2}\mathcal{T}u_m(\mathbf{k}_2)\rangle = -C'_{n,\mathbf{k}_1}C'^*_{m,\mathbf{k}_2}\langle u_n(\mathbf{k}_1)|\hat{\boldsymbol{\nu}}|u_m(\mathbf{k}_2)\rangle^*. \tag{S15}$$

The symmetry properties of the Bloch hamiltonian can also be constrained by other point group symmetries of the crystal. A particularly interesting example is that of mirror symmetry. For example, in the presence of mirror symmetry along the y-axis, such that $\mathcal{M}_yH(\mathbf{k})\mathcal{M}_y^{-1} = H(\mathcal{M}_y\mathbf{k})$, where $\mathcal{M}_y : (x,y) \to (-x,y)$. The energy dispersion thus satisfies $\epsilon_{n,\mathbf{k}} = \epsilon_{n,\mathcal{M}_y\mathbf{k}}$. On the other hand, the velocity operator transforms as $\mathcal{M}_y\hat{\nu}_x\mathcal{M}_y^{-1} = -\hat{\nu}_x$ and $\mathcal{M}_y\hat{\nu}_y\mathcal{M}_y^{-1} = \hat{\nu}_y$. Following similar arguments as above, we obtain symmetry relations for wavefunctions and velocity matrix elements in much the same form as above, leading to distinctive properties of the PD injection and shift photocurrents as discussed in the main text and below.

A. Symmetry analysis for PD injection current

1. Inversion symmetry

When the material possesses $\mathcal{P}$-symmetry and identifying band indices $m,\ n$ in Eq. (S12) with $c,\ v$, we find that the interband velocity matrix element $\boldsymbol{\nu}_{cv}(\mathbf{k},\mathbf{q})$ satisfies $\boldsymbol{\nu}_{cv}(\mathbf{k},\mathbf{q}) = -C^*_{c,\mathbf{k}+\mathbf{q}/2}C_{v,\mathbf{k}-\mathbf{q}/2}\boldsymbol{\nu}_{cv}(-\mathbf{k},-\mathbf{q})$. Thus, for linear [denoted as θ] and circularly [denoted as $\eta=\pm1$] polarised light, the square of the transition matrix element

$$\mathfrak{v}^{\theta(\eta)}_{cv}(\mathbf{k},\mathbf{q}) = |\mathbf{E}^{\theta(\eta)}\cdot\boldsymbol{\nu}_{cv}(\mathbf{k},\mathbf{q})|^2 \tag{S16}$$

thus obeys $\mathfrak{v}^{\theta(\eta)}_{cv}(\mathbf{k},\mathbf{q}) = \mathfrak{v}^{\theta(\eta)}_{cv}(-\mathbf{k},-\mathbf{q})$.

Next we note when the material possesses $\mathcal{P}$-symmetry, the group velocities in valence and conduction bands satisfy $\mathbf{v}_c(\mathbf{k}+\mathbf{q}/2) = -\mathbf{v}_c(-\mathbf{k}-\mathbf{q}/2)$ and $\mathbf{v}_v(\mathbf{k}-\mathbf{q}/2) = -\mathbf{v}_v(-\mathbf{k}+\mathbf{q}/2)$, we have $\boldsymbol{\Delta}(\mathbf{k},\mathbf{q}) = -\boldsymbol{\Delta}(-\mathbf{k},-\mathbf{q})$ odd under $\mathbf{k}\to-\mathbf{k},\ \mathbf{q}\to-\mathbf{q}$. On the other hand, since $\epsilon_{n,\mathbf{k}}$ is even in k-space, we have $\rho(\mathbf{k},\mathbf{q}) = \rho(-\mathbf{k},-\mathbf{q})$.

Therefore, in the presence of inversion symmetry, the injection current (obtained by summing Eq. (3) of the main text over k-space) obeys

$$\partial_t\mathbf{j}^{\rm inj}_\theta(\mathbf{q}) = -\partial_t\mathbf{j}^{\rm inj}_\theta(-\mathbf{q}),\quad \partial_t\mathbf{j}^{\rm inj}_{\rm cir}(\mathbf{q}) = -\partial_t\mathbf{j}^{\rm inj}_{\rm cir}(-\mathbf{q}), \tag{S17}$$

as discussed in Table I of the main text.

2. Time reversal symmetry

When the material possesses $\mathcal{T}$-symmetry, Eq. (S15) gives $\boldsymbol{\nu}_{cv}(\mathbf{k},\mathbf{q}) = -C'_{c,\mathbf{k}+\mathbf{q}/2}C'^*_{v,\mathbf{k}-\mathbf{q}/2}\left[\boldsymbol{\nu}_{cv}(-\mathbf{k},-\mathbf{q})\right]^*$. For linearly polarised light, since $\mathbf{E}^\theta = (\mathbf{E}^\theta)^*$, we have $\mathfrak{v}^\theta_{cv}(\mathbf{k},\mathbf{q}) = \mathfrak{v}^\theta_{cv}(-\mathbf{k},-\mathbf{q})$. In contrast, for circularly polarised light, we have $\mathfrak{v}^\eta_{cv}(\mathbf{k},\mathbf{q}) = \mathfrak{v}^{-\eta}_{cv}(-\mathbf{k},-\mathbf{q})$. This latter relation can be obtained by noting $\mathbf{E}^\eta = (\mathbf{E}^{-\eta})^*$ for circularly polarised irradiation.

We now turn to the carrier velocity $\mathbf{v}_{c(v)}(\mathbf{k})$. For $\mathcal{T}$-symmetry preserving materials, we have $\mathbf{v}_c(\mathbf{k}+\mathbf{q}/2) = -\mathbf{v}_c(-\mathbf{k}-\mathbf{q}/2)$ and $\mathbf{v}_v(\mathbf{k}-\mathbf{q}/2) = -\mathbf{v}_v(-\mathbf{k}+\mathbf{q}/2)$. Thus, the change in carrier velocity obeys $\boldsymbol{\Delta}(\mathbf{k},\mathbf{q}) = -\boldsymbol{\Delta}(-\mathbf{k},-\mathbf{q})$. Similar to that discussed above for inversion symmetry, $\mathcal{T}$-symmetry preserving materials also possess energy dispersion relations that are even in k-space yielding $\rho(\mathbf{k},\mathbf{q}) = \rho(-\mathbf{k},-\mathbf{q})$.

As a result, the linear and circular injection current (obtained by summing Eq. (3) of the main text over k-space) obeys

$$\partial_t\mathbf{j}^{\rm inj}_\theta(\mathbf{q}) = -\partial_t\mathbf{j}^{\rm inj}_\theta(-\mathbf{q}),\quad \partial_t\mathbf{j}^{\rm inj}_{\rm cir}(\mathbf{q}) = \partial_t\mathbf{j}^{\rm inj}_{\rm cir}(-\mathbf{q}) \tag{S18}$$

as discussed in Table 1 of the main text.

Combining both Eq. (S17) and Eq. (S18), we conclude that PD linear injection charge photocurrents are in general allowed in materials with both $\mathcal{P}$- and $\mathcal{T}$-symmetries. In contrast, PD circular injection charge photocurrents (a photocurrent that depends on the helicity of the incident light) vanishes when both $\mathcal{P}$- and $\mathcal{T}$-symmetries in the material remain intact.

3. Mirror symmetry

It is also interesting to consider how point group symmetries can also similarly constrain the form of the PD injection photocurrents. As a simple illustration we focus on PD linear injection photocurrents in a material with a mirror axis along y. For simplicity, we consider the case where incident light (linear) polarization [$\mathbf{E} = E_0\hat{\mathbf{y}}$] as well as non-vertical transition wavevector $\mathbf{q}$ is directed along the mirror axis y. As a result, for $\mathbf{q} = q\hat{\mathbf{y}}$, we have $\mathcal{M}_y\mathbf{q} = \mathbf{q}$. In this case, the square of the transition matrix element obeys $\mathfrak{v}^\theta_{cv}(\mathbf{k},\mathbf{q}) = \mathfrak{v}^\theta_{cv}(\mathcal{M}_y\mathbf{k},\mathbf{q})$. On the other hand, the component of the change in electron group velocity normal to the mirror axis will switch sign $\Delta_x(\mathbf{k},\mathbf{q}) = -\Delta_x(\mathcal{M}_y\mathbf{k},\mathbf{q})$ while the component parallel to the mirror axis remains invariant $\Delta_y(\mathbf{k},\mathbf{q}) = \Delta_y(\mathcal{M}_y\mathbf{k},\mathbf{q})$ under mirror reflection.

We note that $\rho(\mathbf{k},\mathbf{q}) = \rho(\mathcal{M}_y\mathbf{k},\mathbf{q})$ only depends on the energy dispersion (which is even under mirror reflection). As a result, the component of the PD linear injection photocurrent normal to $\mathbf{q}$ (when it is directed along the mirror axis) vanishes: $[\partial_t\mathbf{j}^{\rm inj}_\theta]_x(\mathbf{q}) = 0$, while the component parallel to $\mathbf{q}$ when it is directed along the mirror axis, $[\partial_t\mathbf{j}^{\rm inj}_\theta]_y(\mathbf{q})$,

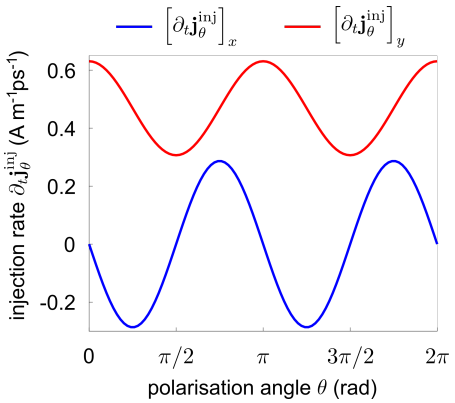

FIG. S1: Polariton drag linear injection photocurrent as a function of light polarisation angle in centrosymmetric BLG. The plasmon polariton wavevector is fixed at $|\mathbf{q}| = 0.03$ nm^{-1}, and all other parameters are the same as Fig. 2 in the main text.

is allowed. This is verified in Fig. S1, which plots the linear injection photocurrent as a function of light polarisation angle θ for a fixed $\mathbf{q}$ along the y-direction (i.e the mirror axis). We observe that the linear injection current flows along the mirror plane when the electric field is polarised along or perpendicular to the mirror plane.

B. Symmetry analysis for PD shift photocurrent

1. *Inversion symmetry*

When the material possesses $\mathcal{P}$-symmetry, the inner product of the wavefunctions follows the relation in Eq. (S11) while the velocity matrix element obeys Eq. (S12). Since all the Bloch wavefunctions in Eq. (S5) occur in pairs (guaranteeing its gauge invariance), the phase factors for the wavefunctions resulting from the $\mathcal{P}$ transformation fully compensate with each other. As a result, we find

$$\mathcal{W}(\mathbf{k}, \delta\mathbf{k}, \mathbf{q}) = -\mathcal{W}(-\mathbf{k}, -\delta\mathbf{k}, -\mathbf{q}), \quad \arg\left[\mathcal{W}(\mathbf{k}, \delta\mathbf{k}, \mathbf{q})\right] = \arg\left[\mathcal{W}(-\mathbf{k}, -\delta\mathbf{k}, -\mathbf{q})\right] + \pi. \tag{S19}$$

Since the shift vector $\mathbf{r}(\mathbf{k}, \mathbf{q})$ depends on the derivative of $\arg\left[\mathcal{W}(\mathbf{k}, \delta\mathbf{k}, \mathbf{q})\right]$, we arrive at

$$\mathbf{R}^{\theta(\eta)}(\mathbf{k}, \mathbf{q}) = -\mathbf{R}^{\theta(\eta)}(-\mathbf{k}, -\mathbf{q}), \tag{S20}$$

where the shift vector flips direction under $\mathbf{k} \to -\mathbf{k},\ \mathbf{q} \to -\mathbf{q}$.

To understand the symmetry properties of the PD shift charge photocurrent, we recall that both $\mathfrak{v}_{cv}^{\theta(\eta)}(\mathbf{k}, \mathbf{q})$ and $\rho(\mathbf{k}, \mathbf{q})$ are even under $\mathbf{k} \to -\mathbf{k},\ \mathbf{q} \to -\mathbf{q}$ [see above]. By summing Eq. (1) of the main text over k-space, we find that the PD shift photocurrents flow in opposite directions for $\pm\mathbf{q}$ in $\mathcal{P}$-preserving materials:

$$\mathbf{j}_\theta^{\rm shift}(\mathbf{q}) = -\mathbf{j}_\theta^{\rm shift}(-\mathbf{q}), \quad \mathbf{j}_{\rm cir}^{\rm shift}(\mathbf{q}) = -\mathbf{j}_{\rm cir}^{\rm shift}(-\mathbf{q}). \tag{S21}$$

as shown in Table I of the main text.

2. *Time reversal symmetry*

Following similar analysis for the injection current, in $\mathcal{T}$-symmetry preserving materials, we have $\hat{\mathbf{e}}_\theta \cdot \boldsymbol{\nu}_{cv}(\mathbf{k}, \mathbf{q}) = -C'_{c,\mathbf{k}+\mathbf{q}/2} C'^{*}_{v,\mathbf{k}-\mathbf{q}/2} \left[\hat{\mathbf{e}}_\theta \cdot \boldsymbol{\nu}_{cv}(-\mathbf{k}, -\mathbf{q})\right]^*$ for linearly polarised light. Combining with the relation for the Bloch wavefunctions in Eq. (S14), we obtain

$$\mathcal{W}^\theta(\mathbf{k}, \delta\mathbf{k}, \mathbf{q}) = -\left[W^\theta(-\mathbf{k}, -\delta\mathbf{k}, -\mathbf{q})\right]^*, \quad \arg\left[\mathcal{W}^\theta(\mathbf{k}, \delta\mathbf{k}, \mathbf{q})\right] = -\arg\left[\mathcal{W}^\theta(-\mathbf{k}, -\delta\mathbf{k}, -\mathbf{q})\right] + \pi. \tag{S22}$$

Here we note that the additional phase factors C' that arise under $\mathcal{T}$ transformation fully compensate each other since the Bloch wavefunctions in Eq. (S5) occur in pairs.

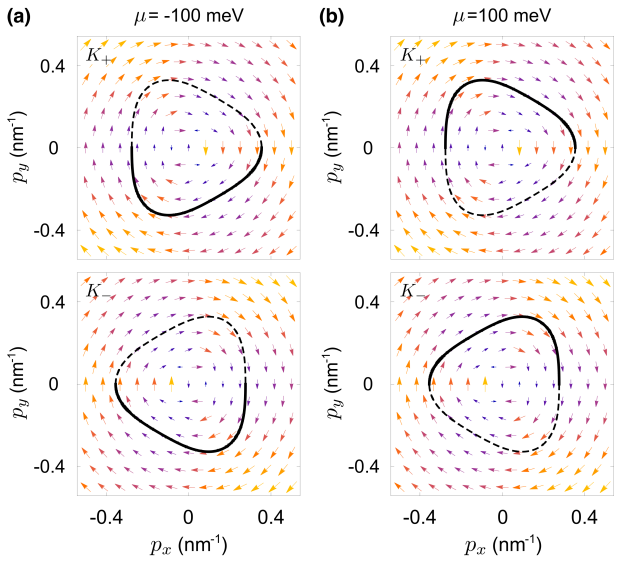

FIG. S2: Polariton selective photoexcitation (PSP) of charge carriers near the Fermi surface for non-vertical interband transitions and circular shift vector. Importantly, PSP yields an imbalanced sampling of shift vector when carriers close to the Fermi surface are excited. Weighted PD circular shift vector $\tilde{\mathbf{R}}^{\zeta,\eta}(\mathbf{p},\mathbf{q})$ for $\eta=+1$ with contour line plots (black) indicating the regions that satisfy energy and momentum conservation. Solid line indicate shift vector regions that are sampled, dashed indicate regions that are not sampled when chemical potential is fixed at $\mu=-\hbar\omega/2$ (a) and $\mu=\hbar\omega/2$ (b) in the K_+ (top panel) and K_- (bottom panel) valleys. Parameters used are the same as Fig. 1 of the main text.

By taking the derivative of the phase of $\mathcal{W}^{\theta}(\mathbf{k},\delta\mathbf{k},\mathbf{q})$, we arrive at the symmetry constraint for the shift vector (for linearly polarized light) in $\mathcal{T}$-preserving materials:

$$\mathbf{R}^{\theta}(\mathbf{k},\mathbf{q})=\mathbf{R}^{\theta}(-\mathbf{k},-\mathbf{q}), \tag{S23}$$

where the shift vector is even under $\mathbf{k}\to-\mathbf{k},\ \mathbf{q}\to-\mathbf{q}$.

On the other hand, for circularly polarised light, we have $\hat{\mathbf{e}}^{\eta}\cdot\boldsymbol{\nu}_{cv}(\mathbf{k},\mathbf{q})=-C'_{c,\mathbf{k}+\mathbf{q}/2}C'^{*}_{v,\mathbf{k}-\mathbf{q}/2}\left[\hat{\mathbf{e}}^{-\eta}\cdot\boldsymbol{\nu}_{cv}(-\mathbf{k},-\mathbf{q})\right]^{*}$. Similarly, the Wilson loop satisfies

$$\mathcal{W}^{\eta}(\mathbf{k},\delta\mathbf{k},\mathbf{q})=-\left[\mathcal{W}^{-\eta}(-\mathbf{k},-\delta\mathbf{k},-\mathbf{q})\right]^{*},\quad \arg\left[\mathcal{W}^{\eta}(\mathbf{k},\delta\mathbf{k},\mathbf{q})\right]=-\arg\left[\mathcal{W}^{-\eta}(-\mathbf{k},-\delta\mathbf{k},-\mathbf{q})\right]+\pi. \tag{S24}$$

As a result, we find that the shift vector (for circularly polarized light with helicity η) satisfies

$$\mathbf{R}^{\eta}(\mathbf{k},\mathbf{q})=\mathbf{R}^{-\eta}(-\mathbf{k},-\mathbf{q}). \tag{S25}$$

By summing Eq. (1) of the main text over k-space, the PD linear and circular shift charge photocurrents in $\mathcal{T}$-symmetric materials obey

$$\mathbf{j}^{\text{shift}}_{\theta}(\mathbf{q})=\mathbf{j}^{\text{shift}}_{\theta}(-\mathbf{q}),\quad \mathbf{j}^{\text{shift}}_{\text{cir}}(\mathbf{q})=-\mathbf{j}^{\text{shift}}_{\text{cir}}(-\mathbf{q}). \tag{S26}$$

Combining with the constraints in Eq. (S21) and (S26), we find that in $\mathcal{P}$- and $\mathcal{T}$-symmetric materials, PD linear shift charge photocurrent vanishes for all non-vertical wavevectors $\mathbf{q}$ while PD circular shift charge photocurrent are allowed.

3. *Mirror symmetry*

Here we illustrate how mirror symmetry can constrain the form of the PD circular shift photocurrent. As a simple illustration we focus on a mirror plane axis along y and consider non-vertical transition wavevector $\mathbf{q}$ directed along the mirror axis y.

For circularly polarised light with polarisation vector $\hat{\mathbf{e}}^{\eta}$, the square of the transition matrix element satisfies $\mathfrak{v}^{\eta}_{cv}(\mathbf{k},\mathbf{q})=\mathfrak{v}^{-\eta}_{cv}(\mathcal{M}_y\mathbf{k},\mathbf{q})$. The Wilson loop obeys

$$\mathcal{W}^{\eta}(\mathbf{k},\delta\mathbf{k},\mathbf{q})=-\mathcal{W}^{-\eta}(\mathcal{M}_y\mathbf{k},\mathcal{M}_y\delta\mathbf{k},\mathbf{q}),\quad \arg\left[\mathcal{W}^{\eta}(\mathbf{k},\delta\mathbf{k},\mathbf{q})\right]=\arg\left[\mathcal{W}^{-\eta}(\mathcal{M}_y\mathbf{k},\mathcal{M}_y\delta\mathbf{k},\mathbf{q})\right]+\pi. \tag{S27}$$

By taking the derivative with respect to $\delta\mathbf{k}$, we have

$$R^{\eta}_{x}(\mathbf{k},\mathbf{q}) = -R^{-\eta}_{x}(\mathcal{M}_y\mathbf{k},\mathbf{q}), \quad R^{\eta}_{y}(\mathbf{k},\mathbf{q}) = R^{-\eta}_{y}(\mathcal{M}_y\mathbf{k},\mathbf{q}). \tag{S28}$$

Since $\rho(\mathbf{k},\mathbf{q}) = \rho(\mathcal{M}_y\mathbf{k},\mathbf{q})$, the y-component of the helicity dependent charge circular shift current vanishes while $\left[\mathbf{j}^{\text{shift}}_{\text{cir}}\right]_x$ is allowed, i.e. PD charge circular shift current in the presence of $\mathcal{M}_y$-symmetry is purely transverse.

III. Giant enhancement of circular shift photocurrent due to PSP

Non-vertical transitions enable polariton selective photoexcitation of charge carriers near the Fermi surface. In particular, when $\mu = \pm\hbar\omega/2$, only half of the interband transition contour (defined by $\delta(\epsilon_{cv}(\mathbf{k},\mathbf{q}) - \hbar\omega)$ can be photoexcited, leading to giant enhancement in photocurrents. As shown by Fig. 1 of the main text, the PD circular shift photocurrents exhibits large and opposite peaks at $\mu = \pm\hbar\omega$. To visualise this PSP induced resonance effect, we plot the distribution of the weighted shift vector $\tilde{\mathbf{R}}^{\zeta,\eta}(\mathbf{p},\mathbf{q}) = \mathfrak{v}^{\zeta,\eta}(\mathbf{p},\mathbf{q})\mathbf{R}^{\zeta,\eta}(\mathbf{p},\mathbf{q})$ [this determines the direction of the PD CS photocurrent, see Eq. (1)] in Fig. S2. Here the interband transition contours (black) indicate $\mathbf{p}$ values that satisfy $\delta(\epsilon^{\zeta}_{cv}(\mathbf{p},\mathbf{q}) - \hbar\omega)$. When $\mu = -\hbar\omega/2$ (in the valence band), the Fermi surface intersects with the interband transition contour so that only the bottom half of the transition contour contributes to the non-vertical interband transitions (solid curve in Fig. S2a). These $\mathbf{p}$ values correspond to occupied carriers in the valence band so that $f_{cv}(\mathbf{p},\mathbf{q}) \neq 0$. In contrast, the other half (dashed curve) do not contribute to the non-vertical interband transitions ($f_{cv}(\mathbf{p},\mathbf{q}) = 0$). This asymmetric sampling of charge carriers on the interband transition contour (enforced by the occupation factors) avoids cancellation of $\tilde{\mathbf{R}}^{\zeta,\eta}(\mathbf{p},\mathbf{q})$ in k-space, leading to large PD CS photocurrents. Similarly, when $\mu = \hbar\omega/2$ is in the conduction band (Fig. S2b), only the top half of the transition contour is available for interband transitions (solid curve in Fig. S2b); these $\mathbf{p}$ values correspond to the region of the conduction band that is unoccupied thus allowing interband transitions ($f_{cv}(\mathbf{p},\mathbf{q}) \neq 0$). Comparing the directions of the weighted shift vector, this yields an PSP enhanced $\mathbf{j}^{\text{shift}}_{\text{cir}}$ that switches sign when the Fermi energy is moved from valence band to the conduction band.

IV. c, v band symmetry and PD photocurrents in bilayer graphene

In this section, we discuss how a symmetry between the conduction c and valence v bands can emerge in the low-energy effective hamiltonian for bilayer graphene. As we will show below, this effective c, v band symmetry leads to a vanishing PD linear injection and circular shift photocurrents at low temperature when the Fermi surface (determined by μ) does not intersect and are far from the interband transition contours (determined by $\hbar\omega$).

We consider the low energy Hamiltonian in Eq. (4) in the main text. For a two-band Hamiltonian, we can directly solve for the eigenenergies and eigenstates. As discussed above, these enable to directly compute the shift vector $\mathbf{r}^{\zeta,\eta}(\mathbf{p},\mathbf{q})$ and the change in carrier velocity $\mathbf{\Delta}^{\zeta}(\mathbf{p},\mathbf{q})$ as a carrier is photoexcited between c and v bands. For the convenience of the reader, we rewrite $H(\mathbf{p})$ as

$$H(\mathbf{p}) = d_1\sigma_x + d_2\sigma_y, \quad d_1 = -\frac{\hbar^2}{2m}(p_x^2 - p_y^2) + \hbar v_3\zeta p_x, \quad d_2 = -\frac{\hbar^2}{m}\zeta p_x p_y - \hbar v_3 p_y. \tag{S29}$$

The energy dispersion is given by $\epsilon^{\zeta}_{c,v}(\mathbf{p}) = \pm\sqrt{d_1^2 + d_2^2}$, where the explicit ζ- and $\mathbf{p}$- dependence of d_1 and d_2 is suppressed for brevity. The corresponding eigenstates are

$$|u^{\zeta}_{c}(\mathbf{p})\rangle = \frac{1}{\sqrt{2}}\begin{pmatrix} e^{-i\phi_{\zeta,\mathbf{p}}} \\ 1 \end{pmatrix}, \quad |u^{\zeta}_{v}(\mathbf{p})\rangle = \frac{1}{\sqrt{2}}\begin{pmatrix} e^{-i\phi_{\zeta,\mathbf{p}}} \\ -1 \end{pmatrix}, \tag{S30}$$

where $\phi_{\zeta,\mathbf{p}} = \tan^{-1}(d_2/d_1)$. As we now show, for $\mathcal{P}$- and $\mathcal{T}$-symmetric bilayer graphene, there is an additional emergent symmetry between the conduction and the valence bands that relates the conduction and valence bands in the separate valleys.

To see this, first we note that (as can be verified by inspection) the energies of the conduction and valence bands in the separate valleys obey $\epsilon^{\zeta}_{c}(\mathbf{p}) = -\epsilon^{\zeta}_{v}(\mathbf{p}) = -\epsilon^{-\zeta}_{v}(-\mathbf{p})$. This emergent c, v band symmetry yields a non-vertical interband transition energy: $\epsilon^{\zeta}_{cv}(\mathbf{p},\mathbf{q}) = \epsilon^{\zeta}_{c}(\mathbf{p}+\mathbf{q}/2) - \epsilon^{\zeta}_{v}(\mathbf{p}-\mathbf{q}/2)$ that obeys

$$\epsilon^{\zeta}_{cv}(\mathbf{p},\mathbf{q}) = \epsilon^{-\zeta}_{cv}(-\mathbf{p},\mathbf{q}) \tag{S31}$$

This symmetry between c and v bands between valleys also constrains the interband velocity matrix elements. Using Eq. (S30), we can explicitly compute $\boldsymbol{\nu}^{\zeta}_{cv}(\mathbf{p},\mathbf{q}) = \langle u^{\zeta}_{c}(\mathbf{p}+\mathbf{q}/2)|\hat{\boldsymbol{\nu}}|u^{\zeta}_{v}(\mathbf{p}-\mathbf{q}/2)\rangle$ [where $\hat{\boldsymbol{\nu}} = \nabla_{\mathbf{p}}H(\mathbf{p})/\hbar$] as

$$\begin{aligned}
\nu^{\zeta}_{cv,x}(\mathbf{p},\mathbf{q}) &= \frac{1}{2}\left(-\frac{\hbar}{m}p_x + v_3\zeta\right)\left[-e^{i\phi_{\zeta,\mathbf{p}+\mathbf{q}/2}} + e^{-i\phi_{\zeta,\mathbf{p}-\mathbf{q}/2}}\right] - \frac{i}{2}\frac{\hbar}{m}\zeta p_y\left[e^{i\phi_{\zeta,\mathbf{p}+\mathbf{q}/2}} + e^{-i\phi_{\zeta,\mathbf{p}-\mathbf{q}/2}}\right] \\
\nu^{\zeta}_{cv,y}(\mathbf{p},\mathbf{q}) &= \frac{1}{2}\frac{\hbar}{m}p_y\left[-e^{i\phi_{\zeta,\mathbf{p}+\mathbf{q}/2}} + e^{-i\phi_{\zeta,\mathbf{p}-\mathbf{q}/2}}\right] - \frac{i}{2}\left(\frac{\hbar}{m}\zeta p_x + v_3\right)\left[e^{i\phi_{\zeta,\mathbf{p}+\mathbf{q}/2}} + e^{-i\phi_{\zeta,\mathbf{p}-\mathbf{q}/2}}\right]
\end{aligned} \tag{S32}$$

We note that when $\zeta \to -\zeta,\ \mathbf{p} \to -\mathbf{p}$, we have $d_1 \to d_1$ and $d_2 \to -d_2$ [see Eq. (S29)]. Thus, $\phi_{\zeta,\mathbf{p}} = -\phi_{-\zeta,-\mathbf{p}}$ is odd in k-space, and we have

$$\boldsymbol{\nu}^{\zeta}_{cv}(\mathbf{p},\mathbf{q}) = \boldsymbol{\nu}^{-\zeta}_{cv}(-\mathbf{p},\mathbf{q}). \tag{S33}$$

As a result, the square of the interband transition matrix for linearly (circularly) polarised light obeys $\mathfrak{v}^{\zeta,\theta(\eta)}(\mathbf{p},\mathbf{q}) = \mathfrak{v}^{-\zeta,\theta(\eta)}(-\mathbf{p},\mathbf{q})$.

The above symmetry relations for how velocity matrix element (and the energies) transform as $\zeta \to -\zeta,\ \mathbf{p} \to -\mathbf{p}$ can be directly used to determine the the PD circular shift photocurrent. To proceed, we consider the shift vector for circularly polarized light reproduced here for the convenience of the reader as

$$\mathbf{R}^{\zeta,\eta}(\mathbf{p},\mathbf{q}) = [\mathbf{A}^{\zeta}_{c}(\mathbf{p}+\mathbf{q}/2) - \mathbf{A}^{\zeta}_{v}(\mathbf{p}-\mathbf{q}/2)] - \nabla_{\mathbf{p}}\arg\left(\mathbf{E}^{\eta}\cdot\boldsymbol{\nu}^{\zeta}_{cv}(\mathbf{p},\mathbf{q})\right) \tag{S34}$$

By direct computation using Eq. (S30), we find the Berry connection in the valence and conduction bands in opposite valleys satisfy $\mathbf{A}^{\zeta}_{c}(\mathbf{p}) = \mathbf{A}^{-\zeta}_{v}(-\mathbf{p})$. This means that the difference of Berry connections [square brackets in Eq. (S34)] is odd when $\zeta \to -\zeta,\ \mathbf{p} \to -\mathbf{p}$, namely: $\mathbf{A}^{\zeta}_{c}(\mathbf{p}+\mathbf{q}/2) - \mathbf{A}^{\zeta}_{v}(\mathbf{p}-\mathbf{q}/2) = -\left[\mathbf{A}^{-\zeta}_{c}(-\mathbf{p}+\mathbf{q}/2) - \mathbf{A}^{-\zeta}_{v}(-\mathbf{p}-\mathbf{q}/2)\right]$. Further, by applying Eq. (S33) to the last term of Eq. (S34) we find: $\nabla_{\mathbf{p}}\arg\left(\mathbf{E}^{\eta}\cdot\boldsymbol{\nu}^{\zeta}_{cv}(\mathbf{p},\mathbf{q})\right)$ is also odd as $\zeta \to -\zeta,\ \mathbf{p} \to -\mathbf{p}$. Hence, due to the emergent c, v band symmetry, we find that as $\zeta \to -\zeta,\ \mathbf{p} \to -\mathbf{p}$ the weighted shift vector $\tilde{\mathbf{R}}^{\zeta,\eta}(\mathbf{p},\mathbf{q}) \equiv \mathfrak{v}^{\zeta,\theta(\eta)}(\mathbf{p},\mathbf{q})\mathbf{R}^{\zeta,\eta}(\mathbf{p},\mathbf{q})$ obeys

$$\tilde{\mathbf{R}}^{\zeta,\eta}(\mathbf{p},\mathbf{q}) = -\tilde{\mathbf{R}}^{-\zeta,\eta}(-\mathbf{p},\mathbf{q}) \tag{S35}$$

This is verified in Fig. S2, which shows the numerical vector plot for $\tilde{\mathbf{R}}^{\zeta,\eta}(\mathbf{p},\mathbf{q})$. Finally, we note that when the Fermi surface is far from any interband transition contours such that $f^{\zeta}_{cv}(\mathbf{p},\mathbf{q})$ is a constant for all $\mathbf{p}$, we have

$$\rho^{\zeta}(\mathbf{p},\mathbf{q}) = \rho^{-\zeta}(-\mathbf{p},\mathbf{q}) \tag{S36}$$

This can be achieved, for instance, for a large $\hbar\omega$ and chemical potential fixed close to charge neutrality at low temperature. In this case, by summing the expression for the PD circular shift photocurrent in Eq. (1) of the main text across all $\mathbf{p}$ and both valleys, we find the PD circular shift photocurrent vanishes due to the emergent symmetry between the valence and the conduction bands.

A similar argument can also be applied to the PD linear injection photocurrent. The change in electron group velocity $\boldsymbol{\Delta}^{\zeta}(\mathbf{p},\mathbf{q})$ can be written as $\boldsymbol{\Delta}^{\zeta}(\mathbf{p},\mathbf{q}) = \nabla_{\mathbf{p}}\epsilon^{\zeta}_{cv}(\mathbf{p},\mathbf{q})/\hbar$. Since $\epsilon^{\zeta}_{cv}(\mathbf{p},\mathbf{q}) = \epsilon^{-\zeta}_{cv}(-\mathbf{p},\mathbf{q})$, we have $\boldsymbol{\Delta}^{\zeta}(\mathbf{p},\mathbf{q}) = -\boldsymbol{\Delta}^{-\zeta}(-\mathbf{p},\mathbf{q})$. In the same fashion as discussed above, when the Fermi surface is far from any interband transition contours such that $f^{\zeta}_{cv}(\mathbf{p},\mathbf{q})$ is a constant for all $\mathbf{p}$, we have Eq. (S36). As a result, in such a situation, applying Eq. (S33), (S36), as well as $\boldsymbol{\Delta}^{\zeta}(\mathbf{p},\mathbf{q}) = -\boldsymbol{\Delta}^{-\zeta}(-\mathbf{p},\mathbf{q})$, and summing the expression for the PD linear injection photocurrent in Eq. (3) of the main text across all $\mathbf{p}$ and both valleys, we find a vanishing PD linear injection current.

This emergent c, v band symmetry can be broken in two ways. As we illustrate in the main text, placing the Fermi energy in the valence band or conduction band in the vicinity of $\pm\hbar\omega/2$ naturally breaks the symmetry between the conduction and the valence band, leading to $f^{\zeta}_{cv}(\mathbf{p},\mathbf{q})$ that is only nonzero for a selective region in the momentum space. This is the polariton selective photoexcitation (PSP) case discussed in the main text. Another way to break the c, v band symmetry is to include a particle-hole asymmetric term in the Bloch Hamiltonian itself, for example, by considering the next-nearest-neighbour hopping in monolayer graphene [17].